JCI The Journal of Clinical Investigation

IRBIT coordinates epithelial fluid and HCO_3^- secretion by stimulating the transporters pNBC1 and CFTR in the murine pancreatic duct

Dongki Yang, … , Katsuhiko Mikoshiba, Shmuel Muallem

J Clin Invest. 2009;119(1):193-202. https://doi.org/10.1172/JCI36983.

Research Article

Fluid and HCO_3^- secretion are vital functions of secretory epithelia. In most epithelia, this entails HCO_3^- entry at the basolateral membrane, mediated by the Na^+-HCO_3^- cotransporter, pNBC1, and exit at the luminal membrane, mediated by a CFTR-SLC26 transporters complex. Here we report that the protein IRBIT (inositol-1,4,5-trisphosphate [IP_3] receptors binding protein released with IP_3), a previously identified activator of pNBC1, activates both the basolateral pNBC1 and the luminal CFTR to coordinate fluid and HCO_3^- secretion by the pancreatic duct. We used video microscopy and ion selective microelectrodes to measure fluid secretion and Cl^- and HCO_3^- concentrations in cultured murine sealed intralobular pancreatic ducts. Short interference RNA–mediated knockdown of IRBIT markedly inhibited ductal pNBC1 and CFTR activities, luminal Cl^- absorption and HCO_3^- secretion, and the associated fluid secretion. Single-channel measurements suggested that IRBIT regulated CFTR by reducing channel mean close time. Furthermore, expression of IRBIT constructs in HEK cells revealed that activation of pNBC1 required only the IRBIT PEST domain, while activation of CFTR required multiple IRBIT domains, suggesting that IRBIT activates these transporters by different mechanisms. These findings define IRBIT as a key coordinator of epithelial fluid and HCO_3^- secretion and may have implications to all CFTR-expressing epithelia and to cystic fibrosis.

IRBIT coordinates epithelial fluid and HCO_3^- secretion by stimulating the transporters pNBC1 and CFTR in the murine pancreatic duct

Dongki Yang,[1] Nikolay Shcheynikov,[1] Weizhong Zeng,[1] Ehud Ohana,[1] Insuk So,[2] Hideaki Ando,[3] Akihiro Mizutani,[3] Katsuhiko Mikoshiba,[3,4] and Shmuel Muallem[1]

[1]Department of Physiology, University of Texas Southwestern Medical Center, Dallas, Texas, USA. [2]Department of Physiology and Biophysics, Seoul National University College of Medicine, Seoul, Republic of Korea. [3]Laboratory for Developmental Neurobiology, Brain Science Institute, RIKEN, Wako, Saitama, Japan. [4]Calcium Oscillation Project, ICORP-SORST, Japan Science and Technology Agency, Wako, Saitama, Japan.

Fluid and HCO_3^- secretion are vital functions of secretory epithelia. In most epithelia, this entails HCO_3^- entry at the basolateral membrane, mediated by the Na^+-HCO_3^- cotransporter, pNBC1, and exit at the luminal membrane, mediated by a CFTR-SLC26 transporters complex. Here we report that the protein IRBIT (inositol-1,4,5-trisphosphate [IP_3] receptors binding protein released with IP_3), a previously identified activator of pNBC1, activates both the basolateral pNBC1 and the luminal CFTR to coordinate fluid and HCO_3^- secretion by the pancreatic duct. We used video microscopy and ion selective microelectrodes to measure fluid secretion and Cl^- and HCO_3^- concentrations in cultured murine sealed intralobular pancreatic ducts. Short interference RNA–mediated knockdown of IRBIT markedly inhibited ductal pNBC1 and CFTR activities, luminal Cl^- absorption and HCO_3^- secretion, and the associated fluid secretion. Single-channel measurements suggested that IRBIT regulated CFTR by reducing channel mean close time. Furthermore, expression of IRBIT constructs in HEK cells revealed that activation of pNBC1 required only the IRBIT PEST domain, while activation of CFTR required multiple IRBIT domains, suggesting that IRBIT activates these transporters by different mechanisms. These findings define IRBIT as a key coordinator of epithelial fluid and HCO_3^- secretion and may have implications to all CFTR-expressing epithelia and to cystic fibrosis.

Introduction

The cardinal function of most secretory glands ductal systems is the secretion of a HCO_3^--rich fluid. Aberrant fluid and HCO_3^- secretion leads to several diseases, including cystic fibrosis (1) and pancreatitis (2). The pancreatic duct epitomizes this function by secreting the bulk of the fluid in the pancreatic juice that contains about 140 mM HCO_3^- and 20 mM Cl^- (3).

Fluid and HCO_3^- secretion requires HCO_3^- entry at the basolateral membrane (BLM) and HCO_3^- exit at the luminal membrane (LM). Basolateral HCO_3^- entry at the pancreatic duct is mediated by the Na^+-HCO_3^- cotransporter, pNBC1 (4–6). Luminal HCO_3^- secretion (efflux) is coupled to Cl^- absorption (influx) and is mediated by the coordinated function of the solute carrier family 26 (SLC26) transporters (SLC26Ts) and the CFTR (7–10). The exact roles of the SLC26Ts and CFTR in mediating Cl^- absorption and HCO_3^- secretion are not well understood. The pancreatic SLC26Ts, SLC26, member 3 (SLC26A3) and SLC26A6, function as coupled Cl^-/HCO_3^- exchangers (8, 11–13), with isoform specific stoichiometry (8, 14). Most models assume that the SLC26Ts mediate the coupled Cl^- absorption and HCO_3^- secretion (3, 15). Indeed, deletion of Slc26a6 in mice inhibited stimulated fluid and HCO_3^- secretion (16).

Although it is clear that CFTR is essential for pancreatic fluid and HCO_3^- secretion, its role in the secretion is less certain. The original model proposed that CFTR-mediated secretion of Cl^- to the duct lumen mainly sustains the Cl^-/HCO_3^- exchange (17). However, several studies showed that CFTR has a limited but significant HCO_3^- permeability (18, 19), which led to the suggestion that CFTR mediates the coupled Cl^- absorption and HCO_3^- secretion. One way to address this important hypothesis is to examine directly the role of CFTR in Cl^- transport in the mouse pancreatic duct. The mouse duct mediates fluid and HCO_3^- secretion in a mechanism similar to that in human and guinea pig ducts (3, 20). However, the mouse duct also mediates HCO_3^--independent fluid secretion that requires basolateral Cl^- influx via the Na^+-K^+-$2Cl^-$ cotransporter isoform 1 NKCC1 (20) and luminal Cl^- efflux by an unknown transporter. In the present work, we took advantage of this activity to demonstrate that the main role of CFTR in the pancreatic duct is Cl^- secretion into the lumen.

An important question concerning the epithelia is how events at the BLM and LM are coordinated to ensure fidelity of the secretory process. A potential coordinator of pancreatic fluid and HCO_3^- secretion is the protein named IRBIT (inositol-1,4,5-trisphosphate [IP_3] receptors binding protein released with IP_3). IRBIT was discovered as a protein that binds to IP_3 receptors (IP_3Rs) (21) and

Conflict of interest: The authors have declared that no conflict of interest exists.

Nonstandard abbreviations used: BLM, basolateral membrane; DIDS, 4,4′-diisothiocyanostilbene-2,2′-disulfonic acid; IP_3, inositol-1,4,5-trisphosphate; IP_3R, IP_3 receptor; IRBIT, IP_3 receptors binding protein released with IP_3; KD, knockdown; LM, luminal membrane; NKCC1, Na^+-K^+-$2Cl^-$ cotransporter isoform 1; NMDG, *N*-methyl-D-glucamine; PDZ, PSD-95/discs large/zona occludens-1; pH_i, intracellular pH; pNBC1, pancreatic Na^+-HCO_3^- cotransporter; siRNA, short interference RNA; SLC26A6, solute carrier family 26, member 6.

Citation for this article: *J. Clin. Invest.* **119**:193–202 (2009). doi:10.1172/JCI36983.

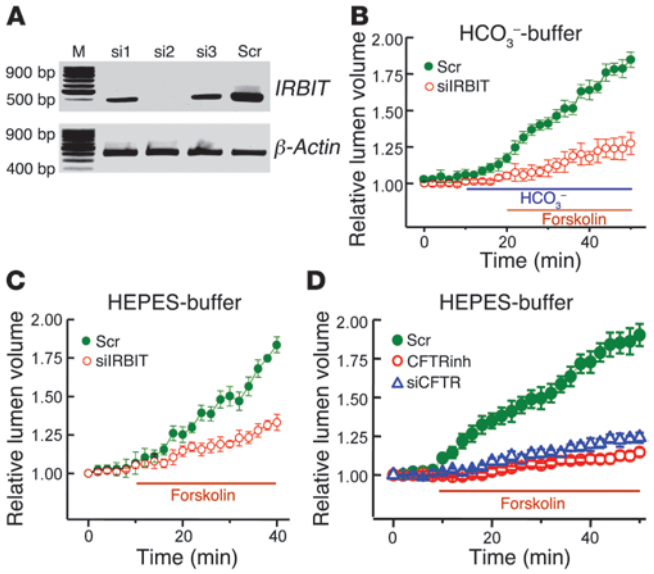

Figure 1

Knockdown of IRBIT inhibits pancreatic duct fluid secretion. (**A**) RT-PCR of *IRBIT* mRNA in sealed ducts treated with scrambled (Scr) or 3 IRBIT dicer siRNA is shown. (**B**) Fluid secretion in ducts perfused in HCO_3^--buffered media and treated with scrambled (filled circles) or IRBIT siRNA (open circles) and stimulated with 5 μM forskolin is shown. Fluid secretion in **C** and **D** was measured as in **B**, except that the ducts were perfused with HEPES-buffered media. (**C**) The ducts were treated with IRBIT dicer siRNA (open circles). (**D**) The ducts were treated with CFTR dicer siRNA (open triangles) or incubated with 10 μM of CFTRinh-172 (CFTRinh, open circles). The results are given as the mean ± SEM of 5–8 experiments.

competes with IP_3 for binding to the IP_3-binding domain of the IP_3Rs to regulate Ca^{2+} signaling (22). IRBIT has several domains (see below): aa 39–43 form a protein phosphatase 1 (PP1) binding ligand, which is followed by PEST (aa 65–92) and coiled-coil domains (aa 111–138), and C terminus PSD-95/discs large/zona occludens-1 (PDZ) ligand (aa 527–530) (23). The PEST domain has 11 serines that can be phosphorylated, and phosphorylation of several serines, including S68, is required for binding of IRBIT to the IP_3Rs (22). However, in vivo only phosphorylation of S68 appears to be regulated by PP1 (23), which inhibits binding of IRBIT to the IP_3Rs.

Recently, it was discovered that IRBIT potently activates pNBC1 but not the kidney-specific isoform kNBC1 (24). IRBIT binds to the N-terminal 1–43 residues of pNBC1 that are not present in kNBC1. Accordingly, when expressed in *Xenopus* oocytes, IRBIT activates pNBC1 but not kNBC1 (24). Phosphorylation of the PEST domain is required for IRBIT binding to and activation of pNBC1 (24). Regulation of pNBC1 by IRBIT suggests that IRBIT may regulate pancreatic fluid and HCO_3^- secretion. Here we show that IRBIT regulates HCO_3^--dependent and, unexpectedly, HCO_3^--independent fluid secretion. This turned out to be due to a prominent activation of CFTR by IRBIT, with IRBIT reducing CFTR closed-duration time to increase channel open probability. Activation of CFTR by IRBIT requires the CFTR PDZ ligand, the IRBIT PEST and coiled-coil domains, and the PDZ ligand. However, deletion of either domain did not prevent interaction of IRBIT with CFTR, suggesting that binding of IRBIT to CFTR is not sufficient for activation of CFTR, and activation of CFTR by IRBIT requires an additional protein that possesses a PDZ ligand. On the other hand, pNBC1 is activated by the IRBIT PEST domain, and the coiled-coil domain and PDZ ligand are not required, indicating that IRBIT activates CFTR and pNBC1 by different mechanisms. The physiological relevance of the regulation of Cl^- absorption and HCO_3^- secretion by IRBIT is demonstrated by marked inhibition of ductal fluid secretion in ducts treated with IRBIT short interference RNA (siRNA). These findings show that IRBIT coordinates pancreatic duct fluid and HCO_3^- secretion and is likely to be a key regulator of epithelial function.

Results

IRBIT regulates both HCO_3^--dependent and HCO_3^--independent pancreatic duct fluid secretion. Intralobular pancreatic ducts in primary culture seal within 12 hours and can be used to measure fluid secretion by measuring the increase in duct lumen volume (25–27). The mouse ducts can be maintained in culture for about 60 hours without loss of polarity or responsiveness and can be treated with dicer siRNA to efficiently silence specific genes (16). We used this system to determine the role of IRBIT in pancreatic duct fluid secretion. The 3 IRBIT dicer siRNA probes tested silence expression of *IRBIT* mRNA, with probe 2 being the most efficient (Figure 1A). This siRNA was used in most experiments, although probe 1 was also shown to have an effect similar to probe 2 on fluid secretion (data not shown), excluding an off-target effects of the siRNA.

Silencing IRBIT expression strongly inhibited the pancreatic duct HCO_3^--dependent fluid secretion (Figure 1B). Since the mouse ducts can also secrete fluid in the absence of HCO_3^- (and thus in a pNBC1-independent manner), we tested the role of IRBIT in this activity, expecting IRBIT not to inhibit this mode of fluid secretion. Unexpectedly, silencing of IRBIT almost abolished the HCO_3^--independent fluid secretion (Figure 1C). Net transepithelial salt transport is obligatory for fluid secretion. The HCO_3^--independent fluid secretion in the mouse is fueled by NKCC1-mediated Cl^- influx across the BLM (20). To identify the mechanism responsible for Cl^- exit across the LM, we examined the role of CFTR in this activity. Silencing of CFTR expression abolished the HCO_3^--independent fluid secretion (Figure 1D). Importantly, inhibition of CFTR channel activity, with the specific CFTR channel inhibitor CFTRinh-172 (28), also inhibited HCO_3^--independent fluid secretion, indicating that the channel function of CFTR is required for this form of fluid secretion.

CFTR mediates pancreatic duct luminal Cl^- secretion. Several models postulate that CFTR mediates, at least part of, ductal coupled Cl^- absorption and HCO_3^- secretion. Comparing Cl^- and HCO_3^- transport by the mouse duct in the presence and absence of HCO_3^- can directly test these postulates and determine the role of CFTR in ductal fluid and electrolyte secretion. For this, we directly measured Cl^- and pH in the lumen of the sealed ducts with ion selective microelectrodes. We held a sealed duct in place with a holding pipette and impaled with a Cl^- selective microelectrode (Figure 2A). Successful impalement of the duct lumen was determined by (a) visual inspection, (b) lower Cl^- in the duct lumen (97 ± 3 mM, n = 78) than in the bath (150 mM), and (c) slow response of the electrodes to changes in bath Cl^- and pH.

Figure 2B shows the effect of HCO_3^- on the pattern of luminal Cl^- changes in the sealed ducts. In HEPES-buffered media, stimulation of the duct with 5 μM forskolin resulted in Cl^- secretion into the duct lumen, with no detectable Cl^- absorption. By contrast, in

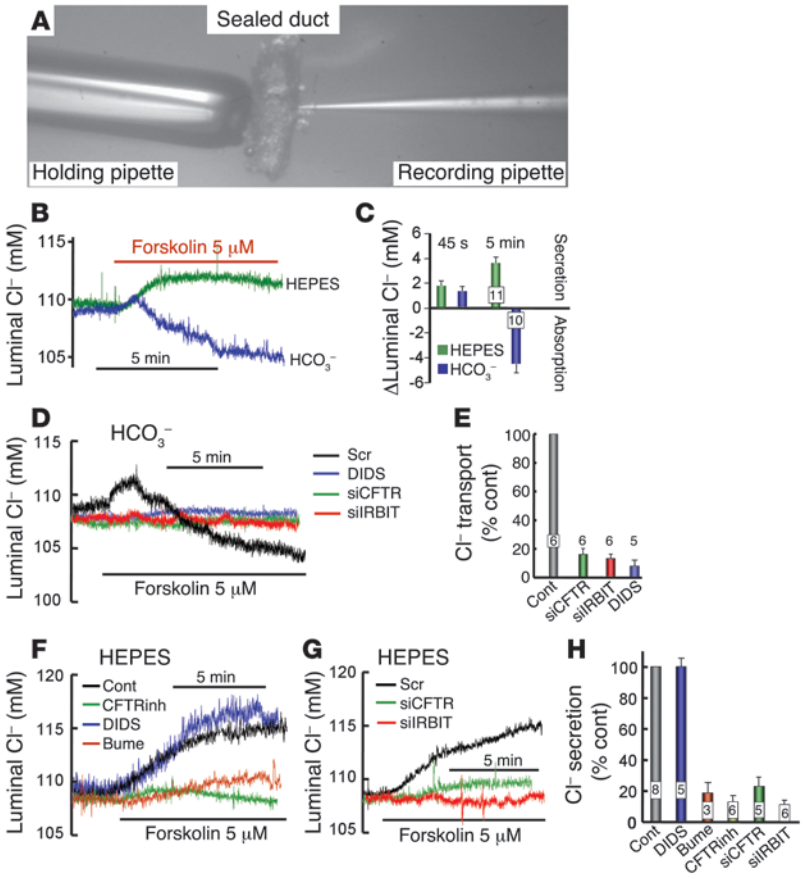

Figure 2
Properties of Cl^- transport by the pancreatic duct. (**A**) A bright-field image of a pancreatic duct held in place by a holding pipette and impaled with a Cl^- recording electrode is shown. Original magnification, ×100. (**B**) The changes in luminal Cl^- of sealed ducts perfused with HEPES-buffered (green trace) or HCO_3^--buffered media (blue trace) are shown. (**C**) The changes in luminal Cl^- concentration after 45 seconds and 5 minutes of stimulation with 5 μM forskolin are summarized (mean ± SEM). (**D**) The changes in luminal Cl^- of sealed ducts perfused with HCO_3^--buffered media (black trace), containing 0.5 mM DIDS to inhibit pNBC1 (blue trace), or treated with CFTR (green trace) or IRBIT (red trace) siRNA are shown. (**E**) Summary (mean ± SEM) of Cl^- secretory activity, as in **D**. Numbers within bars denote number of experiments. (**F**) The changes in luminal Cl^- of sealed ducts perfused with HEPES-buffered media (black trace), containing 0.5 mM DIDS (blue trace), 10 μM CFTRinh-172 (green trace), or 0.1 mM Bumetanide (Bume; brown trace) to inhibit NKKC1 are shown. (**G**) The changes in luminal Cl^- of sealed ducts perfused with HEPES-buffered media and treated with scrambled (black trace), CFTR (green trace), or IRBIT (red trace) siRNA are shown. (**H**) Summary (mean ± SEM) of Cl^- secretory activity, as in **F**. Numbers within bars denote number of experiments. Cont, control.

HCO_3^--buffered media, duct stimulation consistently resulted in a small Cl^- secretion in the first 30–45 seconds that was followed by a large Cl^- absorption from the lumen. The different modes of Cl^- transport in the presence and absence of HCO_3^- (as depicted in the model below) are further illustrated by the inhibition of the HCO_3^--dependent Cl^- absorption by the pNBC1 inhibitor 4,4′-diisothiocyanostilbene-2,2′-disulfonic acid (DIDS) (Figure 2D) and the lack of effect of DIDS on HCO_3^--independent Cl^- secretion (Figure 2F). On the other hand, HCO_3^--independent Cl^- secretion was inhibited by BLM bumetanide, an inhibitor of NKCC1 (Figure 2F). Importantly, Cl^- transport in the presence and absence of HCO_3^- was markedly inhibited by knockdown (KD) of IRBIT (Figure 2, D and G), by KD of CFTR (Figure 2, D and G), and by CFTRinh-172 (Figure 2F).

The findings in Figures 1 and 2 suggest that CFTR-mediated Cl^- secretion is required to support fluid secretion in the presence and absence of HCO_3^-. In the absence of HCO_3^-, the Cl^- is retained in the duct. In the presence of HCO_3^-, shortly after the secretion of Cl^-, Cl^- is absorbed by another HCO_3^--coupled Cl^- transporter. This was further examined by characterizing pancreatic duct HCO_3^- secretion and the role of Slc26a6 in this activity. Although HCO_3^- secretion by the cultured sealed ducts was not robust, it increased in response to forskolin stimulation. After equilibration in HCO_3^--buffered media, ductal HCO_3^- concentration averaged 13.3 ± 1.7 mM and forskolin stimulation increased HCO_3^- concentration to 18.2 ± 3.3 mM. The low level of secretion may reflect in part the relatively low capacity of HCO_3^- secretion by the mouse duct (3), in part, due to the use of intralobular ducts that do not determine the final HCO_3^- concentration in the pancreatic juice, and, in part, due to loss of HCO_3^- secretory capacity by the ducts after 48–72 hours in culture. Nevertheless, ductal HCO_3^- secretion was inhibited by DIDS, CFTRinh-172, KD of CFTR, and KD of IRBIT (Figure 3, A and B). In a previous work, we showed that deletion of the Cl^-/HCO_3^- exchanger Slc26a6 in mice inhibited forskolin-stimulated fluid secretion (16). Notably, deletion of Slc26a6 inhibited forskolin-stimulated HCO_3^- secretion, indicating that Cl^-/HCO_3^- exchange by Slc26a6 is essential for ductal HCO_3^- secretion (Figure 3A). Thus, the findings in Figures 1–3 suggest that ductal HCO_3^- secretion requires the activity of both CFTR and Slc26a6 and that CFTR mainly mediates Cl^- efflux across the LM, while Slc26A6 mediates the bulk of luminal Cl^- absorption and HCO_3^- secretion.

Pattern of IRBIT, CFTR, and IP_3R expression in the pancreatic duct. As indicated above, IRBIT interacts with both the basolateral pNBC1 and the luminal IP_3Rs. By regulating ductal fluid secretion, IRBIT is likely to interact with ion transporters in the apical membrane. Therefore, it was of interest to determine the pattern of expression of IRBIT relative to CFTR and IP_3Rs. This was tested by immunolocalization of IRBIT, CFTR, and IP_3R2 in the pancreatic duct. Since only polyclonal antibodies raised in rabbits and suitable for immunolocalization are available for these proteins, we stained serial pancreatic tissue sections for IRBIT, CFTR, and IP_3R2 (in this order). The images in Figure 3D show that these proteins, including IRBIT, are concentrated in the apical pole. However, clear expression of IRBIT can be observed in the lateral membrane region (Figure 3D, arrows). A survey of several ducts in each of

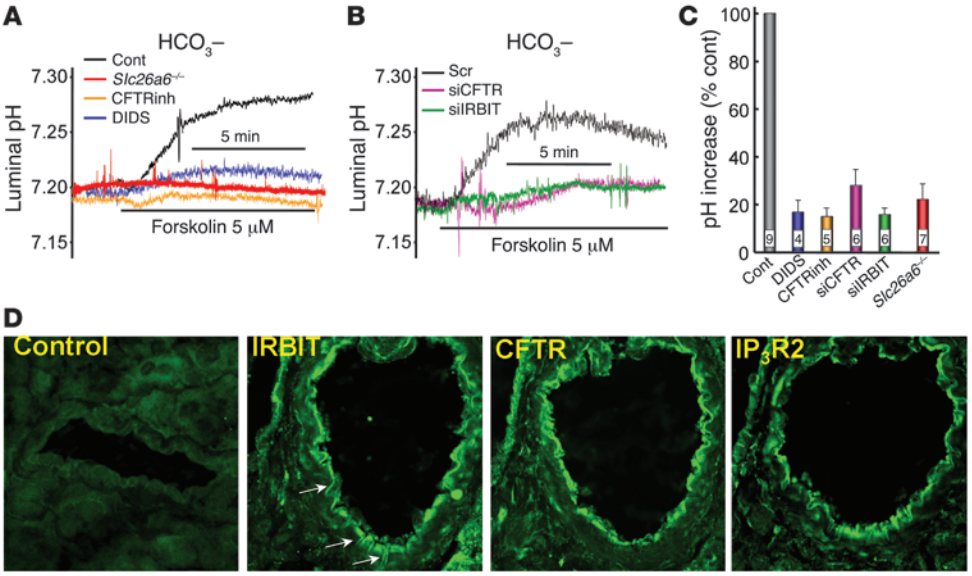

Figure 3

Properties of HCO_3^- secretion by the pancreatic duct. (**A**) The changes in luminal pH of sealed ducts perfused with HCO_3^--buffered media (black trace), containing 0.5 mM DIDS (blue trace), or 10 μM CFTRinh-172 (orange trace) are shown. The red trace shows luminal pH of sealed ducts from *Slc26a6*$^{-/-}$ mice. (**B**) The changes in luminal pH of sealed ducts perfused with HCO_3^--buffered media and treated with scrambled (black trace), CFTR (purple trace), or IRBIT (green trace) siRNA are shown. (**C**) Summary (mean ± SEM) of increase in pH_i, as in **A**. Numbers within bars denote number of experiments. (**D**) Immunolocalization of IRBIT, CFTR and IP_3R2. The first image is the control in which primary antibodies were omitted. Original magnification, ×1,000.

3 experiments revealed expression of IRBIT in the lateral domain, very low if any expression at the basal pole, and prominent concentration at the luminal pole. IRBIT in the lateral pole may regulate pNBC1, while IRBIT in the luminal pole may regulate transporters in this pole, including CFTR. Figure 3D also shows the apical expression of CFTR and IP_3R2, allowing for the possibility of alternate interaction of IRBIT with the 2 proteins.

IRBIT activates native pNBC1 and CFTR. Fluid and HCO_3^- secretion requires stimulation of pNBC1 and/or CFTR by IRBIT, while HCO_3^--independent fluid and Cl^- secretion requires stimulation of NKCC1 and/or CFTR by IRBIT. To test these requirements, we measured the effect of KD IRBIT on ductal pNBC1, NKCC1, and CFTR activities. NKCC1 activity was measured by the NH_4^+ pulse technique (29), in which the cells are exposed to 20 mM NH_4^+. Recovery from the intracellular pH (pH_i) increased in response to NH_3 entry, and its conversion to NH_4^+ is mediated in part by bumetanide-inhibited, NKCC1-mediated NH_4^+ uptake. As shown in Figure 4, A and B, KD of IRBIT has no effect on pancreatic duct NKCC1 activity.

Pancreatic duct pNBC1 activity was measured as the DIDS-sensitive, Na^+- and HCO_3^--dependent recovery from an acid load (5). The ducts were acidified by incubation in Na^+-free, HCO_3^--buffered media, in the presence of a high concentration (10 μM) of the Na^+/H^+ exchange inhibitor S-(*N*-ethyl-*N*-isopropyl) amiloride, to inhibit all ductal Na^+/H^+ exchange activity (30). As shown in Figure 4, C and D, KD of IRBIT inhibited ductal Na^+-HCO_3^- cotransport activity by about 65%. This is in agreement with the 3- to 4-fold stimulation of recombinant pNBC1 by IRBIT (see below and ref. 24).

Ductal CFTR activity was evaluated by measuring forskolin-stimulated Cl^-/NO_3^- exchange. CFTR is highly permeable to NO_3^- (7, 19) and Cl^-/NO_3^- exchange activity, which measures the activity of CFTR, can be measured by the dequenching of the Cl^- dye MQAE fluorescence (7). As shown in Figure 4, E and F, silencing of IRBIT inhibited pancreatic duct Cl^-/NO_3^- exchange by about 70%, suggesting that IRBIT regulates CFTR activity.

IRBIT activates CFTR. To verify and determine the mechanism by which IRBIT activates CFTR, we measured the effect of IRBIT on CFTR channel activity in HEK cells. CFTR Cl^- current was isolated by using Cl^- as the only permeable ion, by stimulating the current with forskolin, and by inhibiting the current with CFTRinh-172. IRBIT was ubiquitous, and when the activity of CFTR was measured by expression in the HEK cells, part of the activity was already stimulated by IRBIT. Hence, the increased CFTR activity due to coexpression of IRBIT and CFTR underestimated the actual stimulatory effect of IRBIT. The full stimulatory effect of IRBIT can be appreciated from comparing the CFTR activity in cells treated with IRBIT dicer siRNA (see below) and cells expressing CFTR and IRBIT (Figure 5). IRBIT increased CFTR current density by about 2-fold when expressed at a CFTR/IRBIT ratio of 1:1 or 1:3 (Figure 5, A and B). This effect is mostly due to activation of CFTR by IRBIT, since IRBIT had no effect on CFTR surface expression, as determined by a biotinylation assay (Figure 5C; $n = 4$).

Single CFTR channel activity measured in cell-attach patches (Figure 5D) shows that IRBIT increased CFTR open probability by about 2.3 fold (Figure 5E). In all 9 experiments with cells expressing CFTR and IRBIT, we could not find a patch with a single channel. Therefore, to determine the principal effect of IRBIT on CFTR channel function, we analyzed open and closed burst durations. IRBIT mainly decreased the mean interburst duration, which translates to a reduction in mean channel close time (Figure 5, F and G).

Multiple IRBIT domains are required for activation of CFTR. IRBIT regulates IP_3Rs by competing with IP_3 for binding to the IP_3 binding site (22). IRBIT activates pNBC1 by interaction with pNBC1(1-43)

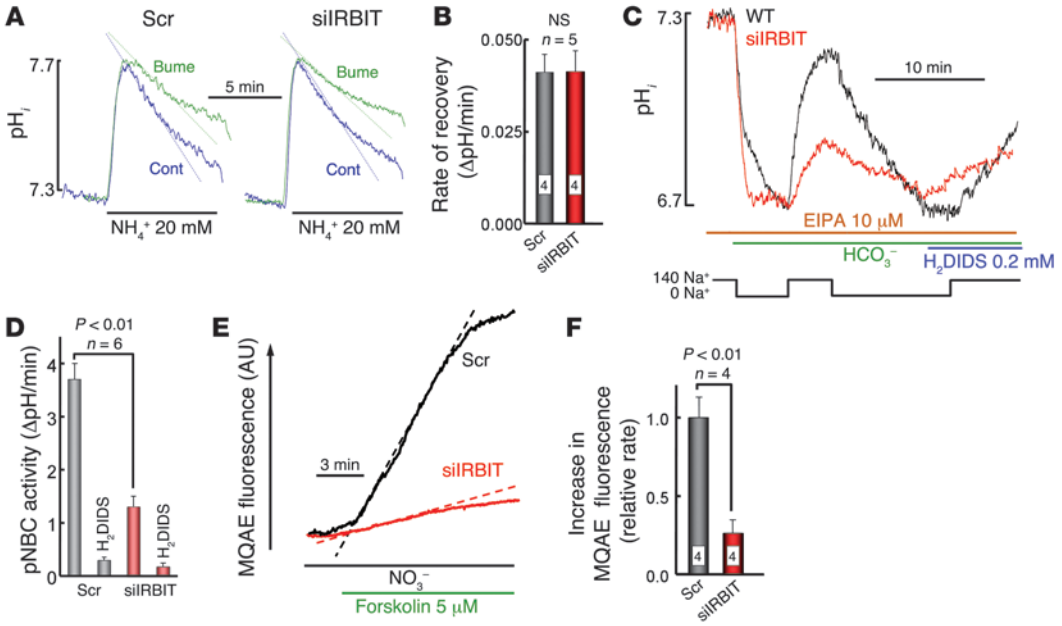

Figure 4

IRBIT stimulates pancreatic duct pNBC1 and CFTR activity. (**A**) Measurement of pH_i in ducts treated with scrambled (left traces) or IRBIT siRNA (right traces) and perfused with HEPES-buffered media is shown. Where indicated the ducts were exposed to media in which 20 mM NH_4Cl replaced 20 mM NaCl, with and without 100 μM bumetanide, as indicated. The inhibition of pH_i recovery by bumetanide is given in **B** in the form of ΔpH/min (mean ± SEM). (**C**) All solutions contained 10 μM S-(*N*-ethyl-*N*-isopropyl) amiloride (EIPA). Ducts treated with scrambled (black trace) or IRBIT siRNA (red trace) in HEPES-buffered media were perfused with Na^+-free HCO_3^--buffered media. After completion of the acidification, the ducts were perfused with media containing 140 mM Na^+ and then were perfused again with Na^+-free media to reacidify the ducts. The ducts were used to measure recovery from acidification in the presence of the pNBC1 inhibitor 0.2 mM H_2DIDS. The rates of Na^+-dependent and H_2DIDS-inhibitable changes in pH_i reflect pNBC1 activity and are summarized in **D**. The results are given as mean ± SEM of 4 experiments. (**E**) The changes in MQAE fluorescence of ducts treated with scrambled (black trace) or IRBIT siRNA (red trace) and perfused in HEPES-buffered media are shown. Where indicated, the ducts were stimulated with forskolin and then perfused with media, in which all Cl^- was replaced with NO_3^-. The dashed lines mark the largest slopes. (**F**) Summary (mean ± SEM) of increase in MQAE fluorescence, as in **E**. Numbers within bars denote number of experiments.

(24). Both interactions are mediated by the IRBIT PEST domain and require phosphorylation of S68 (22, 24). In addition, the last 10 C-terminal residues of IRBIT are required for binding of IRBIT to the IP_3Rs (23, 31). To determine whether IRBIT regulates CFTR by similar interactions, we analyzed binding of CFTR to the IRBIT domains depicted in Figure 6A. When expressed at a 1:1 ratio, CFTR and IRBIT can be readily coimmunoprecipitated. Surprisingly, deletion of any of the IRBIT domains (PEST, C-C, PDZ ligand) (Figure 6A) and the IRBIT(S68A) mutation (data not shown) had no effect on the coimmunoprecipitation. It is necessary to delete the PEST or the coiled-coil domains together with the PDZ ligand of IRBIT to inhibit the coimmunoprecipitation.

The effect of deletion of the IRBIT domains on activation of CFTR is shown in Figure 6, B and C. Notably, even when expressed at a 1:3 CFTR/IRBIT ratio, deletion of the PEST domain, the IRBIT(S68A) mutant, and the last 10 C-terminal residues of IRBIT (IRBITΔ10) or PDZ ligand 4 aa (IRBITΔ4) of IRBIT, which had no effect on the coimmunoprecipitation at a 1:1 expression ratio, nevertheless completely prevented activation of CFTR by IRBIT. Moreover, deletion of the C-C domain (IRBITΔCC) resulted in a dominant negative that inhibited CFTR activity. The specificity of the inhibition was shown by loss of inhibition following deletion of the PDZ ligand (IRBITΔCCΔ4). This was due to a lack of binding of IRBITΔCCΔ4 to CFTR (Figure 6A). Inhibition by IRBITΔCC is likely due to displacement of the native IRBIT from CFTR, since a similar reduction of CFTR current is observed by knockdown of the native IRBIT.

The requirement of the IRBIT PDZ ligand for activation of CFTR raised the question of whether the CFTR PDZ ligand is required for the activation. Deletion of the CFTR PDZ ligand (CFTRΔ4) was sufficient to prevent the coimmunoprecipitation of CFTR with IRBIT and IRBITΔ4 (Figure 6D). Furthermore, as shown in Figure 6, E and F, IRBIT and the IRBIT truncation mutants did not activate CFTRΔ4. Together, the results in Figure 6 suggest that activation of CFTR by IRBIT was facilitated by assembly of the proteins into a complex that was mediated by their PDZ ligands. However, interaction of IRBIT with CFTR was not sufficient for activation of CFTR by IRBIT.

Activation of pNBC1 by IRBIT. To compare the activation of CFTR and pNBC1 by IRBIT, we determined the role of the IRBIT domains on the interaction with and activation of pNBC1. Deletion of the IRBIT C-C domain and the PDZ ligand reduced their binding to pNBC1 (Figure 7A). However, the binding could be restored to near normal levels by increasing the expression of IRBIT truncation mutants by 3 fold. As shown in Figure 7B, deletion of the PEST domain was sufficient to prevent interaction of IRBIT with pNBC1, including at a 1:3 IRBIT/pNBC1 expression ratio. As shown in Figure 7, C (left panel) and D, IRBITΔCC and IRBITΔ4 were not efficient activators of pNBC1 at a 1:1 expression ratio. However, the activation could be rescued by increasing expression of the deletion

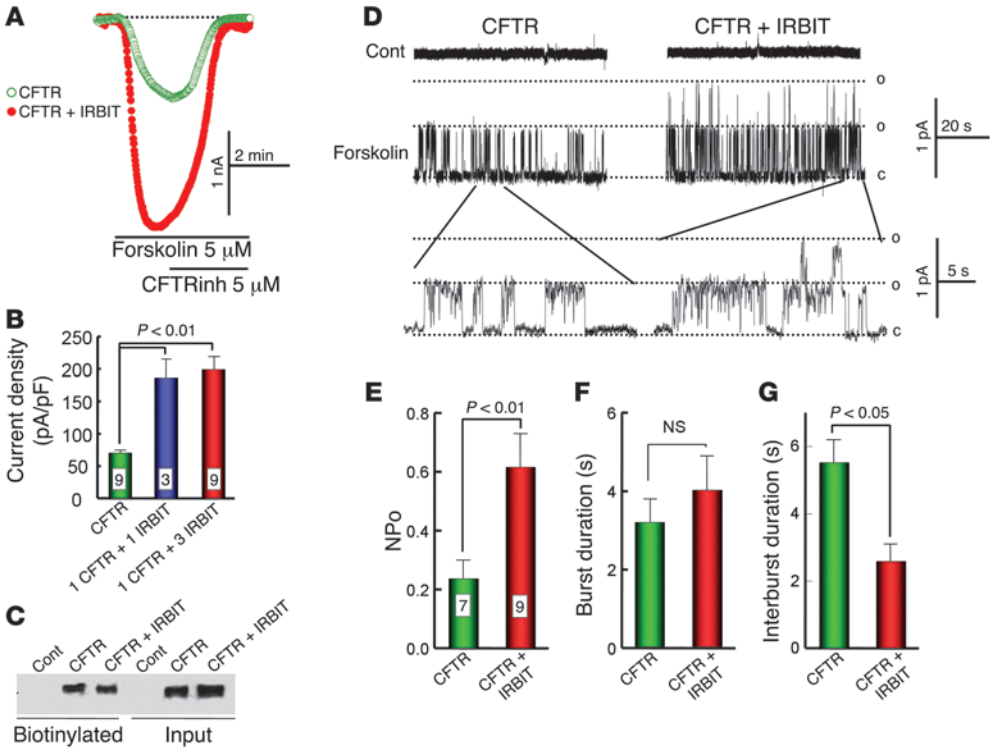

Figure 5
IRBIT activates CFTR. (**A**) The Cl^- current in HEK cells transfected with CFTR (open circles) or CFTR and IRBIT (filled circles) in a 1:3 ratio is shown. Where indicated, the cells were stimulated with forskolin and treated with CFTRinh-172. (**B**) Summary of current density in cells expressing CFTR (green) or CFTR and IRBIT in 1:1 (blue) or 1:3 (red) ratios are shown. Results are given as the mean ± SEM of the number of experiments indicated in the columns. (**C**) The surface expression of CFTR in cells transfected with vector (control), CFTR, or CFTR and IRBIT in a 1:3 ratio, as indicated, is shown. (**D**) Example traces of single CFTR channel activity are shown (c, close channel state; o, open channel state), and (**E**–**G**) show the (mean ± SEM) of (**E**) the open probability (NPo), (**F**) burst duration, and (**G**) interburst duration.

mutants, as shown in Figure 7, C (right panel) and D. Although it does not bind to pNBC1, IRBITΔPEST inhibited pNBC1 activity (Figure 7, C and D). This is likely due to sequestration of the native IRBIT, since knockdown of the native IRBIT similarly reduced pNBC1 activity (Figure 7, C and D). Hence, only the PEST domain is indispensable for activation of pNBC1 by IRBIT, while activation of CFTR by IRBIT requires multiple IRBIT domains.

Discussion

Questions including the role of CFTR and the SLC26 transporters in HCO_3^- secretion and the mechanism by which fluid and HCO_3^- secretion are coordinated are fundamental in epithelial biology. Here we directly measured Cl^- and HCO_3^- secretion into the lumen of sealed ducts to show that the main function of CFTR in the intralobular pancreatic duct is Cl^- secretion. When ducts were bathed in HEPES-buffered media to prevent luminal Cl^- absorption, they secreted Cl^-, and Cl^- secretion required the function of CFTR, as indicated by its inhibition by KD of CFTR and by the inhibitor of CFTR channel activity with CFTRinh-172 (Figure 2). Even when bathed in HCO_3^--buffered media, the ducts initially secreted Cl^-. The subsequent luminal Cl^- absorption required HCO_3^- (Figure 2), and HCO_3^- secretion was inhibited by deletion of the luminal Cl^-/HCO_3^- exchanger Slc26a6 (Figure 3). Together, these findings are consistent with the main function of CFTR at the pancreatic duct is Cl^- secretion, while HCO_3^- secretion is mediated mainly by Slc26a6.

Epithelial fluid and HCO_3^- secretion requires HCO_3^- entry at the BLM and HCO_3^- exit at the LM. However, nothing is known about the mechanism coordinating basolateral HCO_3^- entry with luminal HCO_3^- exit. The present work shows that IRBIT is a master regulator of ductal HCO_3^- secretion, because it activated pNBC1 at the BLM and CFTR at the LM. This is depicted in the model in Figure 8. IRBIT is likely to be recruited to the BLM domain, which expresses pNBC1 by a PDZ domain-containing scaffold, to activate. Activation of pNBC1 is mediated by the IRBIT PEST domain and facilitated by binding of IRBIT and pNBC1 to a scaffolding protein with multiple PDZ domains. At the same time, IRBIT interacts with CFTR to stimulate CFTR channel activity. The PEST and C-C domains are required for interaction of IRBIT with CFTR, but similar to the finding with pNBC1, their interaction also requires or is enhanced by assembly of the proteins into a complex, by a scaffolding protein containing multiple PDZ domains. The nature of the scaffolds mediating IRBIT interaction with pNBC1 and CFTR are not known at the present time. However, several scaffolds have been shown to interact with CFTR (32). A particularly appealing scaffold is PDZK-1/NHERF3, which was isolated by CFTR C terminus affinity purification and has 4 PDZ domains (33) to allow assembly of several proteins in the same complex. It will be of interest to asses the role of PDZK-1 in the regulation of CFTR and pNBC1 by IRBIT. Tight coordination of HCO_3^- entry with HCO_3^- exit increases the fidelity of the secretory process. Significantly, the activation of pNBC1 and CFTR by IRBIT was observed with the native transporters in the pancreatic duct (Figure 4). The physiological importance of the regulation by IRBIT is demonstrated in the almost complete inhibition of ductal Cl^- absorption (Figure 2), HCO_3^- secretion (Figure 3), and the associated fluid secretion (Figure 1) by knockdown of IRBIT.

Another potential role of IRBIT is participation in the synergistic stimulation of fluid and electrolyte transport by cAMP and Ca^{2+}-mobilizing agonists. In CFTR-expressing epithelia, fluid and electrolyte transport is stimulated by cAMP-generating agonists that activate CFTR (3, 34). IP_3-generating and Ca^{2+}-mobilizing agonists can synergistically augment the secretion by an unknown mechanism (3, 34). IP_3 dissociates IRBIT from the IP_3Rs (22). In epithelia, the IP_3Rs

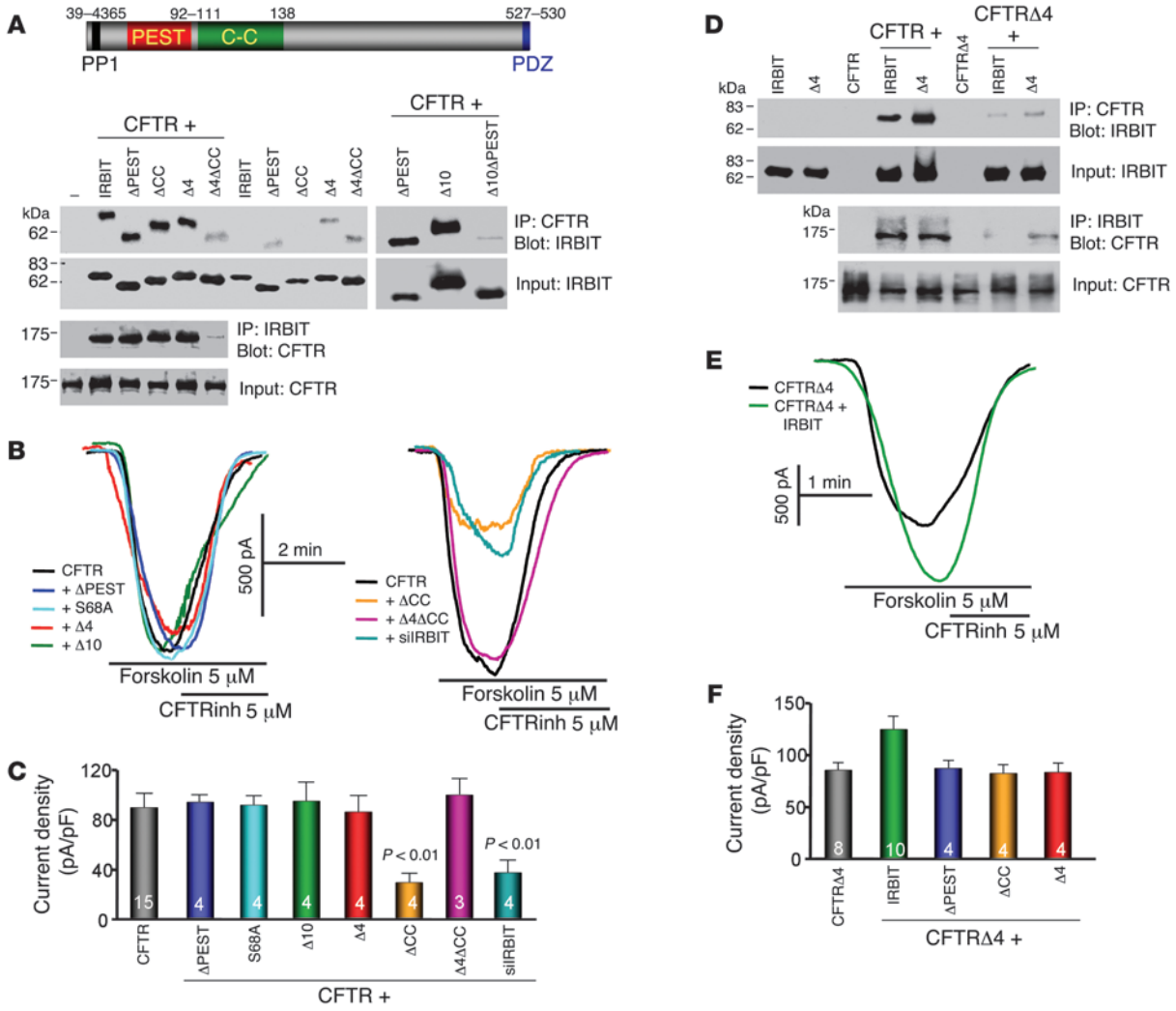

Figure 6

Role of IRBIT domains in interaction with and activation of CFTR. (**A**) A model of the IRBIT domains and the coimmunoprecipitation of IRBIT and CFTR is shown. HEK cells were transfected with a 1:1 ratio of CFTR and the IRBIT truncation mutants or the IRBIT mutants alone (controls) and were used to IP CFTR and blot for IRBIT (upper blots) or IP IRBIT and blot for CFTR (lower blots). ΔCC, IRBITΔCC; ΔPEST, IRBITΔPEST; ΔCCΔ4, IRBITΔCCΔ4. (**B**) Example traces of CFTR current in HEK cells transfected with CFTR and the indicated IRBIT mutants at a 1:3 ratio are shown. The turquoise trace in the right is from a cell treated with IRBIT siRNA. (**C**) The current density calculated in pA/pF (mean ± SEM). The number of experiments is listed on the columns. (**D**) The coimmunoprecipitation of IRBIT and CFTR in cells transfected either with CFTR or with CFTRΔ4 and the indicated IRBIT constructs at a 1:3 ratio are shown. (**E**) Example traces of current measured in cells transfected with CFTRΔ4 or CFTRΔ4 and IRBIT at a 1:3 ratio. (**F**) The current density calculated in pA/pF (mean ± SEM). The number of experiments is listed on the columns.

are clustered and are expressed at a high level just underneath the LM, in which CFTR is expressed (refs. 35–37; Figure 3). It is possible that the IP_3 generated by Ca^{2+}-mobilizing agonists dissociates IRBIT from the IP_3Rs to enhance IRBIT availability and binding to CFTR, thereby augmenting epithelial fluid and electrolyte transport.

A common feature for activation of CFTR (Figure 6) and pNBC1 (Figure 7) and inhibition of the IP_3Rs (23) by IRBIT is that all require the IRBIT PDZ ligand. In addition, all IRBIT effects are mediated by the PEST domain and require phosphorylation of the S68 (refs. 22 and 23; Figure 6). However, it appears that IRBIT affects the activity of the transporters by different mechanisms. The PEST domain interacts with the IP_3-binding domain of the IP_3Rs and with pNBC1(1-43). These domains do not share any homology, and CFTR does not contain a domain homologous to any of these domains. While the PEST domain is sufficient for interaction of IRBIT with the IP_3Rs (22, 23) and pNBC1 (ref. 24; Figure 7), deletion of the PEST domain did not prevent interaction with CFTR (Figure 6). Although deletion of the IRBIT PDZ ligand and C-C domain weakens interaction with pNBC1, they were not required for activation of pNBC1 by IRBIT (Figure 7). By contrast, deletion of the IRBIT PEST and C-C domains and the PDZ ligand had no effect on the interaction with CFTR at a 1:1 expression ratio (Figure 6A); the deletions completely prevented activation of CFTR by IRBIT, even at a 1:3 CFTR/IRBIT expression ratio (Figure 6, C and D). In addition, the IRBITΔCC strongly inhibited CFTR and the inhibition required interaction of IRBITΔCC with CFTR (Figure 6, B and C). Hence, unlike the case with IP_3Rs and pNBC1, interaction of IRBIT with CFTR is not sufficient for activation of CFTR by IRBIT.

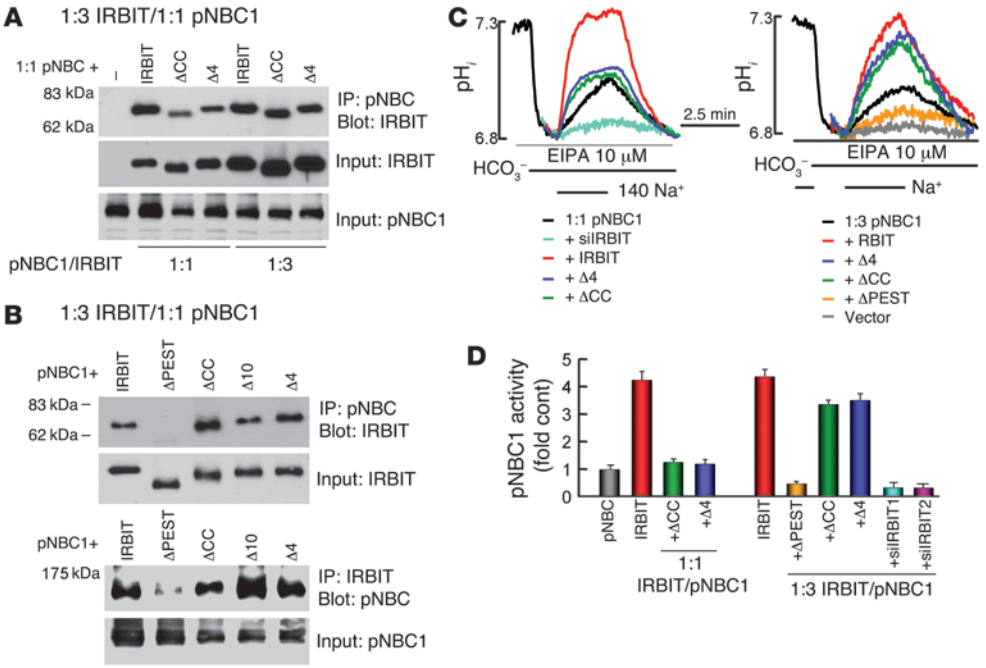

Figure 7
Role of IRBIT domains in interaction with and activation of pNBC1. (**A** and **B**) The coimmunoprecipitation of pNBC1 and the IRBIT truncation expressed at a 1:1 (**A**) or 1:3 (**B**) ratio. –, expressing only pNBC1. (**C**) The effect of IRBIT and the truncation mutants on pNBC1 activity when expressed in a 1:1 (left traces) or 1:3 (right traces) ratio. The turquoise trace is cells treated with IRBIT siRNA and transfected with pNBC1. (**D**) The fold increase of decrease in pNBC1 activity (mean ± SEM).

A potential explanation for the apparent dissociation between the interaction of IRBIT with CFTR and activation of CFTR by IRBIT is that another PDZ ligand-possessing protein is required for the activation of CFTR by IRBIT (modeled in the right side of Figure 8 as protein x). In such a model, IRBIT, CFTR, and the additional protein are assembled into a complex by binding to a PDZ scaffold. CFTR must be present in the complex to allow its activation, since CFTRΔ4 did not interact with (Figure 6D) and was not activated by IRBIT (Figure 6, E and F). IRBITΔ4 retains interaction with CFTR since interaction of IRBITΔ4 with CFTR is mediated by both the PEST and C-C domains, and, therefore, deletion of either the PEST or the C-C domains is not sufficient to disrupt the interaction of IRBIT with CFTR. Deletion of either IRBIT domain may interfere with recruitment of protein X to the complex or its interaction with CFTR that allows activation of CFTR by IRBIT. Irrespective of the exact mechanism by which CFTR and pNBC1 are activated by IRBIT, these activations should have implications for fluid and electrolyte transport by all epithelia that express pNBC1 and CFTR, such as the lung, pancreas, and intestine, and for cystic fibrosis.

Methods

Plasmid construction and solutions. Wild-type CFTR cDNA in pCMV vector was provided by J. Rommens (Hospital for Sick Children, Toronto, Ontario, Canada). pT7TS/pNBC1 was a gift I. Kurtz (UCLA, Los Angeles, California, USA) and the pCDNA3.0/IRBIT and pEGFP-C1/IRBIT constructs were described previously (22). The cDNA encoding pNBC1 and IRBIT were excised from the original vectors and transferred to pEGFP-C1 and p3xFLAG-CMV-7.1. To create all deletion constructs of IRBIT, PCR splicing was performed with pfuTurbo DNA polymerase (Stratagene), using primers to delete specific regions. All constructs were verified by sequencing of the entire open reading frames to ensure lack of unwanted mutations. Polyclonal anti-IRBIT antibodies were prepared in rabbit and were described previously (22). The standard bath solution (solution A) contained 140 mM NaCl, 5 mM KCl, 1 mM $MgCl_2$, 1 mM $CaCl_2$, 10 mM HEPES (pH 7.4 with NaOH), and 10 mM glucose. Na^+-free solutions were prepared by replacing Na^+ with *N*-methyl-D-glucamine (NMDG). HCO_3^--buffered solution (solution B) was prepared by replacing 25 mM Na^+ anion with 25 mM Na^+-HCO_3^- and reducing HEPES to 2.5 mM. HCO_3^--buffered solutions were gassed with 5% CO_2 and 95% O_2. The osmolarity of all solutions was adjusted to 310 mOsmol with the major salt.

Isolation and culture of pancreatic ducts. All euthanasia procedures and experimental protocols with the mice followed NIH guidelines and were approved by the Animal Care and Use Committee of University of Texas Southwestern Medical Center. Cultured, sealed pancreatic ducts from wild-type and *Slc26a6*$^{-/-}$ mice were prepared as described previously (16) by a modification of the method of Ashton et al. (26). In brief, female mice (20–25 g) were killed by cervical dislocation. The pancreas was removed and injected with a digestion buffer consisting of DMEM, containing 50 U/ml collagenase, 400 U/ml hyaluronidase, 0.2 mg/ml soybean trypsin inhibitor (STI), and 2 mg/ml BSA. The tissue was minced and incubated at 37°C for 30 minutes and then in fresh digestion buffer for a further 30 minutes. After a wash with DMEM containing 0.2 mg/ml STI and 3% (w/v) BSA, ducts were microdissected from the partially digested tissue. The ducts were cultured in DMEM supplemented with 10% fetal bovine serum at 37°C and, as indicated, treated with scrambled or the desired siRNA for 48 hours before use.

Analysis of IRBIT gene expression and treatment with dicer siRNA. Total RNA was extracted from microdissected cultured sealed pancreatic ducts using RNeasy Mini Kit from Qiagen. First-strand cDNA was synthesized with the SuperScript Preamplification System (Invitrogen). RT-PCR was performed with appropriate primers, with β-actin as a control cDNA. The optimum

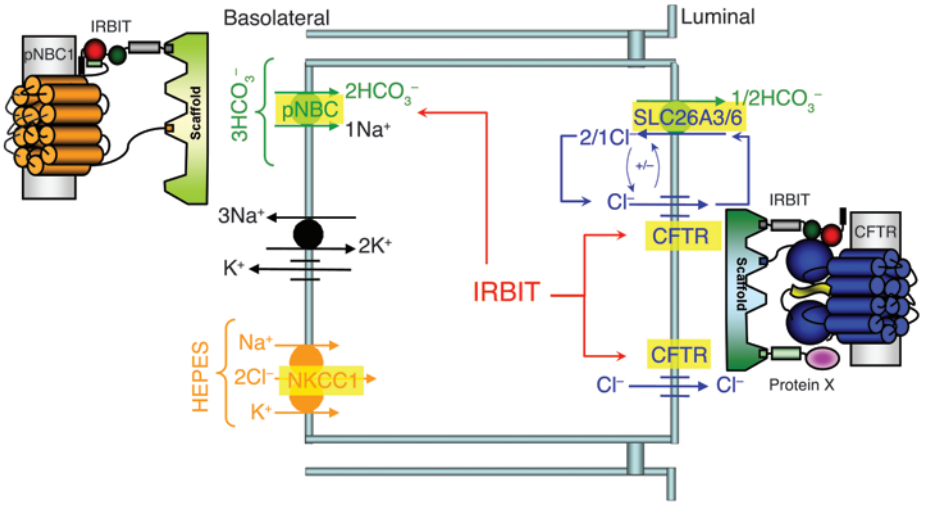

Figure 8
IRBIT coordinates pancreatic duct fluid and HCO_3^- secretion. The model shows the key transporters involved in pancreatic duct fluid and HCO_3^- secretion. IRBIT forms complexes with the BLM pNBC1 and the LM CFTR that are assembled by PDZ domains-containing scaffolding proteins. Activation of pNBC1 and CFTR by IRBIT serves to coordinate HCO_3^- entry at the BLM and HCO_3^- exit at the LM and ensures the fidelity of epithelial fluid and HCO_3^- secretion.

temperature cycling protocol was determined to be 94°C for 1 minute, 50°C for 1 minute, and 72°C for 1 minute for 40 cycles. siRNA treatment was as described previously (16). The IRBIT dicer siRNA sequences used were as follows: siRNA1, GGAGCAAUUGUCUACAUAACAGAAA; siRNA2, CAGAUACUAAUGGACAUAGUACAGT; and siRNA3, AGCAGCAAACCAACUCGAAGGGCAG. The scrambled siRNA was CUUCCUCUCUUUCUCUCCCUUGUGA. Ducts were transfected within 1 hour after dissection and were kept in 35-mm dishes containing 2 ml of DMEM with 10% FBS. In total, 100 pmol siRNA was diluted in 250 μl of Opti-MEM I, and 5 μl Lipofectamine 2000 was diluted in 250 μl of the same medium. The diluted siRNA and Lipofectamine 2000 were mixed and after 20 minutes were added to the dish. After 24 hours, the medium was replaced with a fresh medium without the siRNA, and the ducts were cut in half to release the accumulated fluid and tension. The ducts were used 48 hours after the beginning of the transfection.

Treatment with siRNA and transfection of HEK cells. HEK cells were treated with the 2 siRNA probes used before and validated to markedly reduce IRBIT expression (22). Transfection with scrambled siRNA was used for controls. Transfection with siRNA was exactly as described previously (16). About 48 hours after transfection with the siRNA, the cells were transfected either with CFTR or with pNBC1, and transporters activity was measure 24 hours later.

Immunolocalization. Immunolocalization was performed using the procedures described previously in details (38). In brief, tissue embedded in OCT was used to prepare frozen sections. The sections were permeabilized with 0.5 ml of cold methanol. Nonspecific sites were blocked and the sections were incubated with a 1:1,000 dilution of anti-IRBIT antibodies (22); a 1:2,000 dilution of anti-CFTR antibodies prepared against a C-terminal sequence of CFTR; and a 1:500 dilution of anti-IP_3R2 antibodies (a gift from Ilya Bezprozvanny, University of Texas Southwestern Medical Center). The tissue sections were incubated with the primary antibodies overnight at 4°C and after wash of unbound antibodies, the bound antibodies were detected with goat anti-rabbit IgG tagged with FITC. Images were recorded with a Bio-Rad 1024 confocal microscope.

Measurement of fluid secretion by the sealed ducts. Fluid secretion was measured by video microscopy as described previously (16). The sealed ducts were transferred to a perfusion chamber and perfused with HEPES- and then HCO_3^--buffered media and stimulated with 5 μM forskolin. Images were captured at 2- or 5-minute intervals and analyzed offline by calculating the lumen volume. Due to the variation in size between the microdissected ducts, a normalization procedure was used, with the volume of the first image (V_0) set as 1. Secretion was expressed as the ratio V_t/V_0, which was calculated from the area ratio (A_t/A_0) of the duct, approximating the duct as a cylinder, with A_t as the area at time t and A_0 as the area of the first image and using the equation $V_t/V_0 = (A_t/A_0)^{3/2}$.

Measurement of intraluminal Cl^- and pH in the sealed ducts. Intraluminal Cl^- and pH of the sealed ducts were measured as we described recently (39). In brief, ducts with inner diameters of 40–60 μm were immobilized with large-bore suction pipettes. The lumen was impaled under stereomicroscopic guidance using recording pipettes with 1- to 2-μm tips, filled with the Cl^--sensitive exchanger (477913; Corning) or the H^+ selective resin hydrogen ionophore I, cocktail B (Fluka). The electrodes were calibrated before and after every experiment, and the pH and Cl^- signals were extracted by subtracting the membrane potential signal from the ion selective electrodes signal (40).

pH_i and intracellular Cl^- measurements. pH_i was measured with BCECF (Teflab) by recording BCECF fluorescence at excitation wavelengths of 490 and 440 nm and calibrating the fluorescence as described previously (16). The ducts or HEK cells were loaded with BCECF by 20-minute incubation at room temperature, with 2 μM of BCECF/AM (Teflab). After stabilization of the fluorescence, the cells were perfused with solution A for at least 10 minutes before start of pH_i measurements. Na^+-HCO_3^- cotransport was measured by incubating the ducts and cells with 10 μM S-(*N*-ethyl-*N*-isopropyl) amiloride to inhibit all Na^+/H^+ exchangers (30) and in Na^+-free, HCO_3^--buffered media to acidify the cytosol. Na^+-HCO_3^- cotransport activity was initiated by perfusing the ducts or HEK cells with HCO_3^--buffered media containing 140 mM Na^+. Na^+-HCO_3^- cotransport activity was estimated from the slope of changes in pH_i and is given as ΔpH/min. For intracellular Cl^- measurements, the ducts were loaded with MQAE (Teflab) by 2-hour incubation at 37°C in solution A, containing 5 mM MQAE. After mounting, the ducts were washed and MQAE fluorescence was recorded at an excitation wavelength of 360 nm. To measure Cl^- permeability, the ducts were exposed to solution A, in which Cl^- was replaced with NO_3^-.

Biotinylation and coimmunoprecipitation. For biotinylation experiments, cells were incubated with 0.5 mg/ml EZ-LINK Sulfo-NHS-LC-biotin (Thermo Scientific) for 30 minutes at room temperature, washed with PBS, and lysed. Biotinylated CFTR was isolated with avidin beads and recovered by heating at 37°C for 30 minutes. Extracts were prepared by disruption of cells in ice-cold lysis buffer (20 mM Tris, 150 mM NaCl, 2 mM EDTA, 1% Triton X-100, and a protease inhibitors cocktail), incubation for 15–30 minutes, and collection by centrifugation. For coimmunoprecipitation, extracts were incubated with anti-Flag (M2; Sigma-Aldrich), anti-GFP (Invitrogen), and anti-CFTR (M3A7; Upstate) antibodies. Beads were collected and washed 3 times with lysis buffer, and proteins were recovered by heating in SDS sample buffer.

Current measurement. Whole-cell and single-channel CFTR Cl^- current was recorded as detailed previously (10). The pipette and bath solutions

contained Cl^- as the only permeable anion. The pipette solution contained 150 mM NMDG-Cl, 1 mM $MgCl_2$, 1 mM EGTA, 0.5 mM ATP, and 10 mM HEPES at pH 7.3. The bath solution contained 150 mM NMDG-Cl, 1 mM $MgCl_2$, 1 mM $CaCl_2$ and 10 mM HEPES at pH 7.4. Pipettes had a resistance between 5 and 7 MΩ when filled with pipette solution. Seal resistance was always more than 8 GΩ. Currents were recorded using the Axopatch 200B patch-clamp amplifier (Axon Instruments) at a holding potential of –60 mV, and results were collected at 5 kHz and filtered at 1 kHz. The cell-attached mode was used to record single CFTR channel activity and analyze burst and interburst durations as detailed previously (10) using the method described by Hanrahan et al. (41).

Statistics. Results of all experiments are given as the mean ± SEM of the indicated number of experiments. Significance analysis was performed by ANOVA and *P* values of less than 0.05 were considered significant.

Acknowledgments

We thank Alan Verkman (UCSF) for the gift of CFTRinh-172. This work was supported by the Cystic Fibrosis Foundation grant MUALLE08G0, NIH grants DE12309 and DK38938, and the Ruth Harrell Professorship.

Received for publication July 31, 2008, and accepted in revised form October 15, 2008.

Address correspondence to: Shmuel Muallem, Department of Physiology, Room ND12.300G, University of Texas Southwestern Medical Center, 5323 Harry Hines Blvd., Dallas, Texas 75390-9040, USA. Phone: (214) 645-6008; Fax: (214) 645-6049; E-mail: shmuel.muallem@utsouthwestern.edu.

1. Durie, P.R. 1989. The pathophysiology of the pancreatic defect in cystic fibrosis. *Acta Paediatr. Scand. Suppl.* **363**:41–44.
2. Baron, J.H. 2000. The pancreas. *Mt. Sinai J. Med.* **67**:68–75.
3. Steward, M.C., Ishiguro, H., and Case, R.M. 2005. Mechanisms of bicarbonate secretion in the pancreatic duct. *Annu. Rev. Physiol.* **67**:377–409.
4. Ishiguro, H., Steward, M.C., Lindsay, A.R., and Case, R.M. 1996. Accumulation of intracellular HCO3- by Na(+)-HCO3- cotransport in interlobular ducts from guinea-pig pancreas. *J. Physiol.* **495**:169–178.
5. Zhao, H., Star, R.A., and Muallem, S. 1994. Membrane localization of H+ and HCO3- transporters in the rat pancreatic duct. *J. Gen. Physiol.* **104**:57–85.
6. Abuladze, N., et al. 1998. Molecular cloning, chromosomal localization, tissue distribution, and functional expression of the human pancreatic sodium bicarbonate cotransporter. *J. Biol. Chem.* **273**:17689–17695.
7. Choi, J.Y., et al. 2001. Aberrant CFTR-dependent HCO3- transport in mutations associated with cystic fibrosis. *Nature.* **410**:94–97.
8. Ko, S.B., et al. 2002. A molecular mechanism for aberrant CFTR-dependent HCO(3)(-) transport in cystic fibrosis. *EMBO J.* **21**:5662–5672.
9. Lee, M.G., et al. 1999. Cystic fibrosis transmembrane conductance regulator regulates luminal Cl-/HCO3- exchange in mouse submandibular and pancreatic ducts. *J. Biol. Chem.* **274**:14670–14677.
10. Ko, S.B., et al. 2004. Gating of CFTR by the STAS domain of SLC26 transporters. *Nat. Cell Biol.* **6**:343–350.
11. Melvin, J.E., Park, K., Richardson, L., Schultheis, P.J., and Shull, G.E. 1999. Mouse down-regulated in adenoma (DRA) is an intestinal Cl(-)/HCO(3)(-) exchanger and is up-regulated in colon of mice lacking the NHE3 Na(+)/H(+) exchanger. *J. Biol. Chem.* **274**:22855–22861.
12. Xie, Q., Welch, R., Mercado, A., Romero, M.F., and Mount, D.B. 2002. Molecular characterization of the murine Slc26a6 anion exchanger: functional comparison with Slc26a1. *Am. J. Physiol. Renal Physiol.* **283**:F826–F838.
13. Knauf, F., et al. 2001. Identification of a chloride-formate exchanger expressed on the brush border membrane of renal proximal tubule cells. *Proc. Natl. Acad. Sci. U. S. A.* **98**:9425–9430.
14. Shcheynikov, N., et al. 2006. Regulatory interaction between CFTR and the SLC26 transporters. *Novartis Found. Symp.* **273**:177–186; discussion 186–192, 261–174.
15. Dorwart, M.R., Shcheynikov, N., Yang, D., and Muallem, S. 2008. The solute carrier 26 family of proteins in epithelial ion transport. *Physiology (Bethesda).* **23**:104–114.
16. Wang, Y., et al. 2006. Slc26a6 regulates CFTR activity in vivo to determine pancreatic duct HCO3- secretion: relevance to cystic fibrosis. *EMBO J.* **25**:5049–5057.
17. Sohma, Y., Gray, M.A., Imai, Y., and Argent, B.E. 1996. A mathematical model of the pancreatic ductal epithelium. *J. Membr. Biol.* **154**:53–67.
18. Poulsen, J.H., Fischer, H., Illek, B., and Machen, T.E. 1994. Bicarbonate conductance and pH regulatory capability of cystic fibrosis transmembrane conductance regulator. *Proc. Natl. Acad. Sci. U. S. A.* **91**:5340–5344.
19. Linsdell, P., et al. 1997. Permeability of wild-type and mutant cystic fibrosis transmembrane conductance regulator chloride channels to polyatomic anions. *J. Gen. Physiol.* **110**:355–364.
20. Fernandez-Salazar, M.P., et al. 2004. Basolateral anion transport mechanisms underlying fluid secretion by mouse, rat and guinea-pig pancreatic ducts. *J. Physiol.* **556**:415–428.
21. Ando, H., Mizutani, A., Matsu-ura, T., and Mikoshiba, K. 2003. IRBIT, a novel inositol 1,4,5-trisphosphate (IP3) receptor-binding protein, is released from the IP3 receptor upon IP3 binding to the receptor. *J. Biol. Chem.* **278**:10602–10612.
22. Ando, H., et al. 2006. IRBIT suppresses IP3 receptor activity by competing with IP3 for the common binding site on the IP3 receptor. *Mol. Cell.* **22**:795–806.
23. Devogelaere, B., et al. 2007. Protein phosphatase-1 is a novel regulator of the interaction between IRBIT and the inositol 1,4,5-trisphosphate receptor. *Biochem. J.* **407**:303–311.
24. Shirakabe, K., et al. 2006. IRBIT, an inositol 1,4,5-trisphosphate receptor-binding protein, specifically binds to and activates pancreas-type Na+/HCO3- cotransporter 1 (pNBC1). *Proc. Natl. Acad. Sci. U. S. A.* **103**:9542–9547.
25. Ishiguro, H., et al. 1998. Fluid secretion in interlobular ducts isolated from guinea-pig pancreas. *J. Physiol.* **511**:407–422.
26. Ashton, N., Argent, B.E., and Green, R. 1990. Effect of vasoactive intestinal peptide, bombesin and substance P on fluid secretion by isolated rat pancreatic ducts. *J. Physiol.* **427**:471–482.
27. Ashton, N., Argent, B.E., and Green, R. 1991. Characteristics of fluid secretion from isolated rat pancreatic ducts stimulated with secretin and bombesin. *J. Physiol.* **435**:533–546.
28. Ma, T., et al. 2002. Thiazolidinone CFTR inhibitor identified by high-throughput screening blocks cholera toxin-induced intestinal fluid secretion. *J. Clin. Invest.* **110**:1651–1658.
29. Paulais, M., and Turner, R.J. 1992. Activation of the Na(+)-K(+)-2Cl- cotransporter in rat parotid acinar cells by aluminum fluoride and phosphatase inhibitors. *J. Biol. Chem.* **267**:21558–21563.
30. Lee, M.G., et al. 2000. Na(+)-dependent transporters mediate HCO(3)(-) salvage across the luminal membrane of the main pancreatic duct. *J. Clin. Invest.* **105**:1651–1658.
31. Devogelaere, B., et al. 2006. Binding of IRBIT to the IP3 receptor: determinants and functional effects. *Biochem. Biophys. Res. Commun.* **343**:49–56.
32. Guggino, W.B. 2004. The cystic fibrosis transmembrane regulator forms macromolecular complexes with PDZ domain scaffold proteins. *Proc. Am. Thorac. Soc.* **1**:28–32.
33. Wang, S., Yue, H., Derin, R.B., Guggino, W.B., and Li, M. 2000. Accessory protein facilitated CFTR-CFTR interaction, a molecular mechanism to potentiate the chloride channel activity. *Cell.* **103**:169–179.
34. Melvin, J.E., Yule, D., Shuttleworth, T., and Begenisich, T. 2005. Regulation of fluid and electrolyte secretion in salivary gland acinar cells. *Annu. Rev. Physiol.* **67**:445–469.
35. Lee, M.G., et al. 1997. Polarized expression of Ca2+ channels in pancreatic and salivary gland cells. Correlation with initiation and propagation of [Ca2+]i waves. *J. Biol. Chem.* **272**:15765–15770.
36. Sasaki, T., et al. 1994. Apically localized IP3 receptors control chloride current in airway gland acinar cells. *Am. J. Physiol.* **267**:L152–L158.
37. Yule, D.I., Ernst, S.A., Ohnishi, H., and Wojcikiewicz, R.J. 1997. Evidence that zymogen granules are not a physiologically relevant calcium pool. Defining the distribution of inositol 1,4,5-trisphosphate receptors in pancreatic acinar cells. *J. Biol. Chem.* **272**:9093–9098.
38. Wang, Y., et al. 2006. Sic26a6 regulates CFTR activity in vivo to determine pancreatic duct HCO_3^- secretion: relevance to cystic fibrosis. *EMBO J.* **25**:5049–5057.
39. Shcheynikov, N., et al. 2008. The Slc26a4 transporter functions as an electroneutral Cl-/I-/HCO3- exchanger: role of Slc26a4 and Slc26a6 in I- and HCO3- secretion and in regulation of CFTR in the parotid duct. *J. Physiol.* **586**:3813–3824.
40. Shcheynikov, N., et al. 2006. Coupling modes and stoichiometry of Cl-/HCO3- exchange by slc26a3 and slc26a6. *J. Gen. Physiol.* **127**:511–524.
41. Hanrahan, J.W., et al. 1998. Patch-clamp studies of cystic fibrosis transmembrane conductance regulator chloride channel. *Methods Enzymol.* **293**:169–194.